Remote Sensing of Environment 176 (2016) 308–319

Contents lists available at ScienceDirect

Remote Sensing of Environment

journal homepage: www.elsevier.com/locate/rse

Assessing the transferability of statistical predictive models for leaf area index between two airborne discrete return LiDAR sensor designs within multiple intensely managed Loblolly pine forest locations in the south-eastern USA

Matthew Sumnall [a,*], Alicia Peduzzi [b], Thomas R. Fox [a], Randolph H. Wynne [c], Valerie A. Thomas [d], Bruce Cook [e]

[a] Virginia Polytechnic Institute and State University, Department of Forest Resources and Environmental Conservation, 228 Cheatham Hall (Mail Code: 0324), Blacksburg, VA 24061, USA
[b] United States Dept. of Agriculture — Forest Service, 507, 25th Street, Ogden, UT 84401, USA
[c] Virginia Polytechnic Institute and State University, Department of Forest Resources and Environmental Conservation, 319 Cheatham Hall (Mail Code: 0324), Blacksburg, VA 24061, USA
[d] Virginia Polytechnic Institute and State University, Department of Forest Resources and Environmental Conservation, 307A Cheatham Hall (Mail Code: 0324), Blacksburg, VA 24061, USA
[e] NASA Goddard Space Flight Center, Biospheric Sciences Laboratory, Code 618, Greenbelt, MD 20771, USA

ARTICLE INFO

Article history:
Received 19 February 2015
Received in revised form 18 January 2016
Accepted 4 February 2016
Available online 16 February 2016

Keywords:
Loblolly pine
Forest management
LiDAR
Remote sensing
Leaf area index

ABSTRACT

Leaf area is an important forest structural variable which serves as the primary means of mass and energy exchange within vegetated ecosystems. The objective of the current study was to determine if leaf area index (LAI) could be estimated accurately and consistently in five intensively managed pine plantation forests using two multiple-return airborne LiDAR datasets. Field measurements of LAI were made using the LiCOR LAI2000 and LAI2200 instruments within 116 plots were established of varying size and within a variety of stand conditions (i.e. stand age, nutrient regime and stem density) in North Carolina and Virginia in 2008 and 2013. A number of common LiDAR return height and intensity distribution metrics were calculated (e.g. average return height), in addition to ten indices, with two additional variants, utilized in the surrounding literature which have been used to estimate LAI and fractional cover, were calculated from return heights and intensity, for each plot extent. Each of the indices was assessed for correlation with each other, and was used as independent variables in linear regression analysis with field LAI as the dependent variable. All LiDAR derived metrics were also entered into a forward stepwise linear regression. The results from each of the indices varied from an R^2 of 0.33 (S.E. 0.87) to 0.89 (S.E. 0.36). Those indices calculated using ratios of all returns produced the strongest correlations, such as the Above and Below Ratio Index (ABRI) and Laser Penetration Index 1 (LPI1). The regression model produced from a combination of three metrics did not improve correlations greatly (R^2 0.90; S.E. 0.35). The results indicate that LAI can be predicted over a range of intensively managed pine plantation forest environments accurately when using different LiDAR sensor designs. Those indices which incorporated counts of specific return numbers (e.g. first returns) or return intensity correlated poorly with field measurements. There were disparities between the number of different types of returns and intensity values when comparing the results from two LiDAR sensors, indicating that predictive models developed using such metrics are not transferable between datasets with different acquisition parameters. Each of the indices were significantly correlated with one another, with one exception (LAI proxy), in particular those indices calculated from all returns, which indicates similarities in information content for those indices. It can then be argued that LiDAR indices have reached a similar stage in development to those calculated from optical-spectral sensors, but which offer a number of advantages, such as the reduction or removal of saturation issues in areas of high biomass.

Published by Elsevier Inc.

1. Introduction

The surface area of the foliated elements within the forest canopy is the primary surface which controls the processes of canopy-gas exchange, such as photosynthesis (Duchemin et al., 2006), evaporation (Cleugh, Leuning, Mu, & Running, 2007), transpiration (Chen, Chen, Ju, & Geng, 2005), rainfall interception (Chen et al., 2005), and carbon flux (Leuning, Cleugh, Zegelin, & Hughes, 2005). This biophysical parameter is typically assessed though leaf area index (LAI), which can be defined as the ratio of half of the total leaf surface area per unit of ground area, and for coniferous species which have cylindrical needles, the projected or hemi-surface area of the needles per unit of ground area (Chen & Black, 1992). As a result LAI varies with hydrological,

* Corresponding author.

http://dx.doi.org/10.1016/j.rse.2016.02.012
0034-4257/Published by Elsevier Inc.

biochemical, and biophysical processes, either due to natural stand development of forest management practices (e.g. initial site treatment, thinning, fertilization and vegetation control). Given the role of LAI in determining many forest ecosystem processes, several techniques have been developed to rapidly estimate LAI.

The most common methods used for estimating LAI across the landscape-scale rely on the empirical relationships between LAI and various manipulations of spectral information from airborne or spaceborne imagery. The estimates of LAI from such imagery can be complicated by variation in the properties of the solar radiation reflected from the earth's surface which can be attenuated by atmospheric attributes (e.g. water vapor), and land cover properties (e.g. understory vegetation, senescent leaves, shadows) which can alter the spectral signature of the surface type (Erikson, Eklundh, & Kuusk, 2006), in addition to the mixing of signatures (Bioucas-Dias, Plaza, & Dobigeon, 2012). A drawback of optical imagery is that it is that it is appropriate for examining horizontally distributed features only.

More recently, numerous methods have been developed for the analysis of datasets obtained through Light Detection and Ranging (LiDAR) to estimate a suite of forest biophysical characteristics. Airborne small-footprint LiDAR remote sensing, with high point densities, can characterize both horizontal and vertical structures within forested environments. The use of LiDAR has rapidly come into prominence in estimating forest characteristics, such as canopy height, basal area, timber volume, and biomass (Evans, Hudak, Faux, & Smith, 2009), through the use of regression methods using LiDAR derived metrics related to the return vertical distribution and intensity of LiDAR returns over a range of scales and locations (Anderson et al., 2008; Lefsky, Cohen, Parker, & Harding, 2002; Lim, Treitz, Baldwin, Morrison, & Green, 2003a; Lim, Treitz, Wulder, St-Onge, & Flood, 2003b; Maltamo et al., 2005; Næsset, 2002). The derivation of individual tree metrics is possible using small-footprint laser data with a sufficient point density (e.g. Kaartinen et al., 2012).

There is an increasing body of research attempting to use the three-dimensional structural information from LiDAR to estimate LAI based on statistical methods. Many small footprint LiDAR systems are capable of recording multiple discrete returns per laser pulse (e.g. between one and five returns). Whilst LiDAR derived statistical models have found similar relationships between dependent and independent variables for many examples of forest inventory metrics, each model is calibrated and validated against local field data. Reliable models which can be transferred to other locations are unfortunately lacking. In addition many of the LiDAR derived predictors are often highly correlated, which can bias model estimates (Field, 2013).

The majority of LAI ground measurements used for validation of remote sensing data is based on indirect optical and non-destructive measurements. Due to the methods in deriving LAI from such techniques, a common variable used is effective LAI, which is related to gap fraction, and differs from 'true' LAI because the leaves or needles are not randomly distributed within the canopy and can be clumped within shoots. Effective LAI also includes the areas of branches and stems (Stenberg, 1996). As in Solberg et al. (2009) According to Beer–Lambert law, the effective LAI might be derived for a given forest vertical position from the number of LiDAR pulses to pass through that point, and expressed as:

$$LAI_e = \beta \times \ln\left(P^{-1}\right) \quad (1)$$

where LAI_e is the effective LAI, β is the slope parameter to be predicted, and P is number of pulses. There are a number of examples of LiDAR derived indices or ratios of first, last and single returns, intended to emulate Eq. (1), being produced in the related research (e.g. Morsdorf, Kötz, Meier, Itten, & Allgöwer, 2006; Korhonen, Korpela, Heiskanen, & Maltamo, 2011; Solberg et al., 2009; Zhao & Popescu, 2009), and regressing them against effective LAI over a variety of forest types.

A number of challenges related to the differences in LiDAR sensor design and acquisition parameters exist. As pulse penetration properties and return frequency distribution can differ between LiDAR acquisitions (Naesset, 2009; Hopkinson, 2006), the proportions of first-of-many, single and last returns will differ when comparing systems capable of detecting differing types of returns. Another issue prevalent in discrete return LiDAR, is the 'blind spot' following each detected return (up to 1.2–5 m), during which nothing can be detected (Reitberger, Krzystek, & Stilla, 2008). The usage of LiDAR intensity remains a contested issue due to the proprietary methods that commercial sensors use to report return intensity which can change in flight, making it impossible to directly compare two discrete returns (Lim et al., 2003a). These issues may be symptomatic of locational or data acquisition specific differences pose problems to the transferability of LiDAR based LAI models.

A number of studies have attempted to assess multiple LiDAR derived indices or statistical predictive models against one another. One such example is Richardson, Moskal, and Kim (2009), where four previously published LAI predictive models were assessed for prediction accuracy for a number of locations within Washington State, USA. The results varied in terms of R^2 values from 0.49–0.66, which was lower than in the original studies. The differences in estimates were ascribed to differences in vegetation types, LAI ranges and LiDAR acquisition parameters within each of the studies. The research outlined in Hopkinson and Chasmer (2009) assessed four LiDAR derived indices of fractional cover across seven study areas within Canada, with acquisitions from two generations of Optech airborne laser scanning systems. The authors report R^2 values for predictions between 0.70–0.78, with the highest correlations existing for indices produced from the sum of intensity values from both the ground or canopy vertical elements relative to the total for all study sites.

The aim of the current study was to test a number approaches for estimating LAI in homogenous coniferous forest with various management treatments and understory vegetation conditions, covering a wide range of LAI values. The specific objectives were to: (1) estimate LAI over multiple locations and sensor designs/acquisition parameters through a number of modeling approaches, and (2) evaluate the modeling approaches for estimating LAI from airborne discrete return LiDAR.

2. Materials and methods

2.1. Study sites

A total of five study sites were visited which are located within North Carolina and Virginia, USA, were used for the current research project. The initial three sites were established in 2008 and maintained in support of research studies investigating the role of intensive management in optimizing Loblolly pine (*Pinus taeda* L.) production. These studies were a joint effort between the Forest Productivity Cooperative (FPC) (http://forestproductivitycoop.net/), academic institutions, the USDA Forest service, the Virginia Department of Forestry and private industry.

The first of these sites was the RW195501 trial (RW19), which is part of a region wide study examining the effects fertilization and thinning in mid-rotation stands. This trial is located in the Piedmont of Virginia in Appomattox County at 37° 26′ 32″ N and 78° 39′ 43″ W. A total of 32 plots were installed in a 13 year old stand. The plots vary in size from approximately 400 to 1280 m^2 and could be of a square or rectangular shape. At the time of the LiDAR acquisition in summer 2008, only plots had been established and no additional silvicultural techniques had been applied besides the traditional forest operational practices used in the area.

The second site in Virginia, was the RW180601 (RW18), which was also part of a region wide study designed with the objective of understanding the optimal rates and frequencies of nutrient additions for rapid growth in young stands. The trial was located in the Piedmont site of Virginia, Brunswick County at 36° 40′ 51″ N and 77° 59′ 13″ W. A total of 40 plots were installed in 1999 in a 6 year old planted stand. These plots had complete weed control and five nutrient treatments, as follows: 0, 67, 134, 201, and 269 kg/ha nitrogen (N) applied with

phosphorous (0.1 × N). Nutrient application frequencies were at 1, 2, 4 and 6 year intervals. Thirty plots were thinned in 2008. Plot size varied from approximately 400 to 470 m^2, and again could be of a square or rectangular shape.

The third site was the Southeast Tree Research and Education Site (SETRES), and was located in sand hills of North Carolina, in Scotland County, at 34° 54′ 17″ N and 79° 29′ W. This trial was established in 1992 in an 8 year old plantation. The goal of the study was to quantify the effects of nutrient and water availability on above and below ground productivity and growth efficiency in Loblolly pine. Treatments consisted of nutrient additions (nitrogen, phosphorus, potassium, calcium and magnesium), and irrigation. See Albaugh et al. (1998) for a complete description of site and treatment. Plot size was 900 m^2 (30 × 30 m), 4 blocks and 4 plots per block, for a total of 16 plots.

Two final study sites were located in North Carolina, USA, and enumerated in 2013. Both sites are managed in support of research studies for the production of Loblolly pine. The first of the sites was established at Parker Tract (Parker) (35° 48′ N, 76° 40′ W) is managed by the USDA forest service for research on climate response, water availability and ecosystem stress (more information can be found at: http://www.nrs.fs.fed.us/data/lcms/tpt/). Understory vegetation was not managed and was present in high density across the whole site. The site was planted in 1992 and thinned in 2009 removing approximately 50 to 60% of the pine biomass. The total site extent was approximately 1.4 × 0.9 km. Eight field plots were installed throughout the site with a plot size of 15 × 15 m (225 m^2).

The second study site was established at the Loblolly pine plantation areas located in Duke Research Forest (Duke) (35° 57′ N 79° 05′ W) which is managed for research and teaching purposes by Duke University. The Duke Forest site is composed of a mix of coniferous and deciduous stands. The site is managed to provide a diversity of stand types and age-class distributions over a variety of soils and topographic conditions. Silvicultural practices can include may include prescribed burning, disking, pre-commercial and commercial thinning, various regeneration and harvest systems, planting, herbicide application, and fertilization. The sites visited varied in planting date from 1981 to 2005, and covered an extent of 3.3 × 2.0 km (more information can be found at: http://dukeforest.duke.edu/). The understory in pure stands is often sparse, but in mixed or old stands, it is dominated by native hardwoods. A total of twenty field plots were installed throughout the location with a plot size of 15 × 15 m (225 m^2).

2.2. Field estimates of leaf area index

LAI data was collected using the LiCOR LAI-2000 Plant Canopy Analyzer on each plot during later summer (September 7–19, 2008) with the exception of the RW19 trial, which was measured in January 2009. Above canopy readings were recorded remotely every 15 s by placing the instrument in an open field adjacent to the stand during the same data and time that measurements were taken inside the stand. All within stand measurements were made at a height of 1 m above ground, and facing upwards regardless of the presence of understory or mid-story vegetation. Due to the instruments design all measurements were recorded under diffuse sky conditions at dawn and dusk periods, to ensure the sensor only recorded indirect light. The above and below canopy instruments always faced north with a 90° view cap, with the sensor directed upwards. Sampling points were distributed equally along a transect. Two transects were recorded for each plot, one close to the edge of the plot and the other in the middle of the plot, with a total of 14–25 readings being taken based on plot dimensions.

As LAI measurements for the RW19 location were measured in January 2009, a regression model was produced to generate approximate summer 2008 values. The model was developed using effective LAI LiCOR measurements made in summer (August) 2005 and winter (February) 2006 from 17 plots (100 × 100 m) established in 7 and 10 year old Loblolly pine stands. See Peduzzi, Wynne, Thomas, et al. (2012a and 2012b) for more information.

The 2013 field plots were visited between the 23rd and 27th of October. Field LAI was assessed using the LiCOR LAI-2200 Plant Canopy Analyzer on each plot. Above and below canopy readings were recorded as stated previously. Measurements were made at 1.25 m above ground height. Two transects were used, one along the tree row at the center of the plot and the second in the gap between rows. Measurements were taken every systematically along the transect, with 30 readings being taken per plot.

The calculation of effective LAI per plot was produced through the LiCOR FV-2000 or FV-2200 software, for data acquired in 2008–9, and 2013, respectively. Plot-level readings were averaged, where ring number 5 measurements were masked to reduce error introduced by the stem and branches of the coniferous trees. Records with transmittance values >1 were skipped in order to avoid bad readings that can alter mean values per plot. The above and below canopy readings were matched by time (Welles & Norman, 1991). Estimates of effective LAI were calculated, with no clumping corrections applied, i.e. assuming a random distribution of the components within the canopy. The LAI values for each site are summarized in Table 1.

2.3. LiDAR data

Small footprint discrete-return LiDAR was acquired for each of the three study areas in 2008. The systems were an Optech ALTM 3100. The system could record multiple returns (1–4) with a sampling density of 5 pulses per meter square. The flying altitude was approximately 1200 m with a pulse repetition frequency of 70 kHz. The laser operated at 1064 nm with a beam divergence of approximately 0.3 mrad. The scan angle was less than 15°. Instrument vertical accuracy over bare ground was 15 cm and horizontal accuracy is 0.5 m. The LiDAR return intensity was not calibrated and was recorded as integer values between 0 and 255.

Small-footprint discrete-return LiDAR data were acquired for both 2013 study sites coincident with field data capture. The data was provided by the NASA G-LiHT team (further information can be found in Cook et al. (2013)). The scanning LiDAR system was a Riegl VQ-480. The flying altitude was approximately 610 m with a pulse repetition frequency of 150 kHz, recording up to 6 returns per pulse. The approximate pulse density was 6 per meter-square. The laser operated at 1550 nm with a beam divergence of 0.3 mrad. The scan angle was less than 10°. The instruments accuracy over bare ground was 0.25 cm. The LiDAR return intensity was not calibrated and was recorded as an integer value between 0 and 65,535.

Preprocessing steps were required before metrics could be derived from the LiDAR data for analysis. Each of these steps was performed using the RSC Lastools software (Armston, 2014). Ground elevation returns were classified through a progressive morphological filter as outlined in Zhang et al. (2003). LiDAR return above ground heights were calculated by subtracting the corresponding ground point heights, interpolated into a surface (nearest neighbor method), from the original (unclassified) dataset.

All LiDAR returns which intersected within field plot horizontal extents were clipped from the datasets, and metrics generated utilizing the R statistical software (version 3.1.1.) (http://www.r-project.org/). A suite of LiDAR metrics were calculated based on the distribution of all points and vegetation points (i.e. >0.2 m). Ground points were defined as those returns ≤0.2 m above ground height. The following metrics were generated for both all and canopy returns: the mean, median, standard deviation, variance, coefficient of variation, skewness and kurtosis (as in: Falkowski, Evans, Martinuzzi, Gessler, & Hudak, 2009; Hudak, Crookston, Evans, Hall, & Falkowski, 2008). Percentiles were calculated for all returns at 5% increments (5, 10…90, 95%) for the proportion of returns. Metrics related to LiDAR return intensity were computed from a single flight line for each plot. The flight line providing the largest

Table 1
A summary of the LAI values recorded for the five study sites.

Study site	Number of field plots	LAI measurement height (m)	LAI mean	LAI standard deviation	LAI minimum	LAI maximum
RW18 (2008)	40	1.0	1.56	1.30	0.45	4.85
RW19 (2008)	32	1.0	2.56	0.27	1.93	3.05
SETRES (2008)	16	1.0	2.52	0.47	1.55	3.27
Duke (2013)	20	1.25	3.88	1.09	2.24	5.39
Parker Tract (2013)	8	1.25	3.20	0.63	2.24	4.11

number of returns incident within the plot extent was selected and metrics were calculated for the coefficient of variation, skewness and kurtosis for all returns and canopy returns. Canopy density slices, using a modified approach outlined in Peduzzi et al. (2012b), were also computed. These metrics were computed above and below the mode of vegetation returns. Ten 1 m sections were (5 above and 5 below the mode based upon the maximum value of a histogram of the number of returns against height) were classified and metrics generated from the slices corresponding to the proportion of total returns, average height of returns, standard deviation, variance, coefficient of variation, skewness and kurtosis. All of these metrics are summarized in Table 2.

In addition to these point cloud summary statistics, other related research studies have examined the use of LiDAR for obtaining estimates of LAI or fractional cover by directly inferring it from a pulse return ratio or the number of canopy-to-total returns (e.g. Barilotti, Turco, Napolitano, & Bressan, 2005; Hopkinson & Chasmer, 2009; Morsdorf et al., 2006; Solberg et al., 2009). These indices can be related to the principles used by field instruments to indirectly measure LAI on the ground (measuring the solar light transmission or reflectance through the vegetation). The main difference between the canopy interaction of solar and airborne LiDAR laser pulse radiation is geometric. Solar radiation can be incident across a wide range of zenith angles if its temporal and latitudinal distribution is considered, while LiDAR pulses are typically incident at near overhead (0–30°) angles. Any direct LiDAR sampling will be biased towards overhead for a path length close to the height of the canopy, which implies LiDAR estimates maybe directly related to leaf area index.

Each of these indices is based on the frequency or cumulative return intensity of contact of laser pulse returns from within the forest vegetation. These indices use a vertical stratification to define 'ground' and producing a ratio of returns form the remaining or complete vertical profile or a ratio of different return types or sum of intensity. The ground return threshold was set to the same as the height which LAI measurements were taken in the field, i.e. 1.0 m above ground for 2008 data and 1.25 m for 2013, as the measurement height was found to be of importance in Sumnall et al. (2016). As before, indices calculated from LiDAR intensity were derived from a single flight line (i.e. the flight line providing the largest number of returns incident within the plot extent). Intensity inputs for these indices correspond to the sum of intensity values from all returns. A summary of each of the indices is provided in Table 3. Two additional indices were constructed, the first was based upon the Above and Below Ratio Index (ABRI) which used the cumulative intensity of returns above and below the 'ground' return threshold ($ABRI_{int}$). And the second is a modification of the Light Penetration Index presented in (Barilotti et al., 2005), which uses the sum of intensity of returns below the ground return threshold divided by the sum of intensity from all returns. This index is referred to as $LPI3_{int.all}$.

Table 2
A summary of LiDAR point cloud return height and intensity distribution metrics for each plot level area.

LiDAR metrics	Symbols
All returns	All_{max}, All_{mean}, All_{median}, All_{stdev}, All_{cv}, All_{skew}, All_{kurt}, All_{5th}…All_{95th}.
Vegetation returns	Veg_{max}, Veg_{min}, Veg_{mean}, Veg_{median}, Veg_{stdev}, Veg_{cv}, Veg_{skew}, Veg_{kurt}, Veg_{5th}…Veg_{95th}.
Number of laser pulses	Grd_{pulses}, Veg_{pulses}, All_{pulses}.
Proportion of returns	R_i = total number of *i* returns/R_{All} *i* = first, last, single and intermediate returns
Crown density slices around mode of vegetation returns	CDi, CDi_{mean}, CDi_{stdev}, CDi_{CV}, CDi_{skew}, CDi_{kurt} CDi = [number of returns in *i* divided by all returns] (*i* = +1, +2, +3, +4, +5, 0, −1, −2, −3, −4, −5) *i* = +1… + 5 at *i* meters above vegetation mode *i* = mode of vegetation returns *i* = −1…−5 at *i* meters below vegetation mode
Intensity value summary from all returns	$I.ALL_{CV}$, $I.ALL_{skew}$, $I.ALL_{kurt}$
Intensity value summary from vegetation returns	$I.Veg_{CV}$, $I.Veg_{skew}$, $I.Veg_{kurt}$

2.4. Statistical analysis

A dataset of combining all 116 field plot LiDAR summary metrics were computed and combined with field based LAI measurements. Statistical analyses were conducted in R. Each of the thirteen indices was tested in bivariate regression against field estimates of LAI in order to assess the predictive power of each. Multiple stepwise regression analysis was performed between the field measurements of effective LAI and all of the LiDAR derived indices and those metrics summarized in Table 2. This was to determine if supplementary data could improve the univariate LAI estimation models, or provide a better correlation using different metrics.

Several criteria were used to examine potential models including R^2 and adjusted R^2. Once a potential model was produced a more rigorous assessment was applied, that included individual covariate significance (Type III error *t* tests, $p \leq 0.05$); absence of multicollinearity (i.e. variance inflation factor ≤ 1, Bowerman & O'Connell, 1990) and residual homoscedasticity. Each of the model covariates were examined for contribution to R^2 value, significance, individual standard error and variance inflation factor values, and removed as necessary and the stepwise procedure re-implemented. Model validity in multiple linear regression relies partly on the number of observation and covariates. Adjusted R^2 is more conservative that R^2, thus models where the two were showed little change were sought. Those models which exhibited a combination of the lowest changes of R^2 to adjusted R^2 and lowest overall dataset standard error, whilst still satisfying individual covariate criteria, was preserved as the final model.

A bivariate correlation matrix was produced in order to determine which of the indices, listed in Table 3, are linearly related to each other. Pearson correlation coefficients were produced for each of the bivariate comparisons. A specific directional relationship between the variables is unknown, therefore two-tailed significance tests were applied.

3. Results

3.1. Testing the individual LiDAR indices

The best fit regression results comparing the rings 1–4 LAI 2000/2200 measurements for each of the field plot locations are summarized in Table 4, which summarizes R^2, standard error and regression

Table 3
Computation of LiDAR indices. Where R_{grd} is the number of returns below the ground threshold (e.g. 1 m). R_{veg} is the number of return above the 'ground' threshold. R_{All} is the total number of returns. Where $R\ldots_{first}$ is the number of first of many returns (e.g $R_{grd,first}$ is the sum of ground first returns), $R\ldots_{last}$ is the number of last returns, $R\ldots_{single}$ is the number of single returns, and $R\ldots_{pulses}$ is the total number of pulses. *Int* denotes the sum of return intensities from LiDAR returns, e.g. Int_{all} is the sum of intensity of all returns, Int_{grd} is the sum of intensity for returns below the ground threshold, whereas Int_{veg} is the sum of intensity. $Int\ldots_{inter}$ is the sum of intensity from intermediate returns (i.e. between first and last).

Index	LAI range	Forest types	Calculation
LAI proxy (LAI_{PROXY}) (Morsdorf et al., 2006)	0.1–1.9	Mountain pine (*Pinus mugo* subsp. *uncinata*) and stone pine (*Pinus cembra*)	$LAI_{proxy} = \frac{R_{Veg.First}}{R_{Veg.last}+R_{Veg.single}}$
Laser penetration index 1 ($LPI1$) (Barilotti et al., 2005 as cited in Peduzzi et al., 2012b)	0.79–4.47	Loblolly pine	$LPI1 = \frac{R_{grd}}{R_{all}}$
Laser penetration Index 2 ($LPI2$) (Solberg et al., 2009)	0.58–5.13	Norway spruce (*Picea abies*)	$LPI2 = \frac{R_{grd.single}+0.5(R_{grd.first}+R_{grd.last})}{R_{grd}+0.5(R_{first}+R_{last})}$
First echo Cover Index (FCI) and Last echo Cover Index (LCI) (Korhonen et al., 2011)	0.15–4.61	Norway spruce and Scots pine (*Pinus sylvestris*)	$FCI = \frac{R_{veg.single}+R_{veg.first}}{R_{All.single}+R_{All.first}}$ $LCI = \frac{R_{veg.single}+R_{veg.last}}{R_{All.single}+R_{All.last}}$
Above and Below Ratio Index ($ABRI$) (Sumnall et al., 2016)	1.39–5.42	Loblolly pine	$ABRI = \frac{R_{veg}}{R_{grd}}$
Fractional cover (multiple) (Hopkinson & Chasmer, 2009)	0.18–4.2	Thirteen coniferous and deciduous species	$FC1_{all} = \frac{R_{veg}}{R_{all}}$ $FC2_{Int.first} = \frac{Int_{veg.first}}{Int_{all.first}}$ $FC3_{Int.all} = \frac{Int_{veg}}{Int_{all}}$ $FC4_{Beerslaw} = 1-\left(\frac{\left(\frac{Int_{grd.single}}{Int_{all}}\right)+\sqrt{\frac{Int_{grd.last}}{Int_{all}}}}{\left(\frac{Int_{first}+Int_{single}}{Int_{all}}\right)+\sqrt{\frac{Int_{inter}+Int_{last}}{Int_{all}}}}\right)$
ABRI changed to use the sum of return intensity ($ABRI_{int}$)			$ABRI_{Int} = \frac{Int_{veg}}{Int_{grd}}$
A modified Light Penetration Index ($LPI3_{int.all}$) to use the sum of return intensity from below ground threshold			$LPI3_{Int.all} = \frac{Int_{grd}}{Int_{all}}$

equation constant and coefficient values. Four of the regression analyses were found to contain non-linear relationships. Thus, a quadratic transform was applied to $FC1_{all}$, square root transforms were applied to the $LPI1$ and $LPI2$ and a $\log_{10}$ transform to $ABRI$ variables.

In terms of the index metrics generated from the sum of LiDAR return numbers, five of eight models produced high R^2 values (>0.75). The regression analysis applied to the LAI_{PROXY} calculation produced very low R^2 values (i.e. <0.1) indicating there is very little if any correlation between the index and LAI within this context. The FCI model produced a relatively low R^2 value of 0.432 and RMSE of 0.796, nearly double that of the five remaining models. These five models produced similar R^2 and standard error values overall, and were all significant ($p < 0.05$), which the exception of the $FCI1_{all}$ constant (or intercept) term within the regression model was not significant when assessed with the student's t test (i.e. $p > 0.05$).

The graphs of predicted LAI against measured LAI for those models derived from the number of returns are presented in Fig. 1, excluding LAI_{PROXY}. The graphs for sqrt($LPI1$) and sqrt($LPI2$) both depict a linear trend well. It should be noted, however, that LAI values at the upper extents of the LAI range, (approximately >4) are underestimated for $LPI2$. The values for the FCI poorly estimate LAI values beyond the average 2–3 LAI value. It is possible to observe a number of groupings within the graph which correspond to the records from individual study sites, for example records for the RW19 and SETRES study sites appear separate from the rest. Elements of which also appear to link with those from Duke and Parker Tract, which may indicate other potential populations. The graph for the LCI predictions depict an overall linear trend, and as before poorly represent LAI estimates at the minimum and maximum of the range. It should also be noted, however, that there is also a relative increase in values for records derived from 2013 data (Duke and Parker) in comparison to those from 2008. The remaining two indices $\log_{10}(ABRI)$ produced a linear trend well and produced the lowest standard error value (slightly lower than sqrt($LPI1$)). The $FC1^2_{all}$ model, when compared to those derived from the LPI1 and ABRI does not predict LAI values at the extents of the LAI range encountered here, i.e. where LAI is <1 and >5.

Table 4
Regression statistics for each of the LiDAR derived indices tested. Note that the '*' denotes the Students t-test result was significant (i.e. $p < 0.05$).

Model	Non-linear transform (y/n)	R^2	Standard error	Constant	Coefficient
LiDAR return frequency					
LAI_{PROXY}	n	0.066	1.033	3.384*	−1.803
$sqrt(LPI1)$	y	0.885	0.362	8.159*	−9.276
$sqrt(LPI2)$	y	0.858	0.403	7.084*	−7.789
FCI	n	0.432	0.805	−1.049*	4.388
LCI	n	0.811	0.464	0.146	5.258
$\log_{10}(ABRI)$	y	0.886	0.360	1.641*	3.861
$(FC1_{all})^2$	y	0.882	0.367	−0.029	6.374
LiDAR intensity					
$FC2_{int.first}$	n	0.331	0.874	0.655 *	2.882
$FC3_{int.all}$	n	0.447	0.795	0.234	4.372
$FC4_{beerslaw}$	n	0.475	0.774	0.127	5.656
$ABRI_{int}$	n	0.435	0.803	1.416 *	0.810
$LPI3_{int.all}$	n	0.449	0.793	0.587 *	6.041

The regression models calculated from the sum of return intensity values were all poor when compared to those described above ($R^2 < 0.5$) with higher RMSE values. For both $FC3_{int.all}$ and $FC4_{beerslaw}$ the constant (or intercept) terms within the regression model were not significant when assessed with the student's t test (i.e. $p > 0.05$). The graphical representations of these models are presented in Fig. 2. LAI values which occupy the extremities on the range of 0–6 are not well predicted in all cases. The predictions presented in Fig. 2 show similar distributions to that of the FCI in Fig. 1, where the RW19 and SETRES datasets collected in 2008 are separate from the other records. The records presented for $ABRI_{int}$ may indicate two separate non-linear distributions.

3.2. Consideration of plot area

Plot size varied a great deal between the five study sites, it was therefore necessary to explore how this affected the modeled values of LAI. The LAI estimates were organized by field plot area, and separated into similar groups, these were: (i) 225 m^2 ($n = 28$) and 300–399 m^2 ($n = 3$); (ii) 400–499 m^2 ($n = 45$); (iii) 600–699 m^2 ($n = 8$); (iv) 700–799 m^2 ($n = 8$); (v) 900 m^2 ($n = 16$); (vi) 1200–1299 m^2 ($n = 8$). RMSE was calculated for each group, the results of which are presented in Fig. 3. The five indices, $LPI1$, $LPI2$, LCI, $ABRI$ and FC_{all}, appear relatively stable for all six area size classes. The LAI_{PROXY}, FCI and all intensity indices show a similar pattern of higher error relative to the other five indices, but also larger error when plot size is smaller.

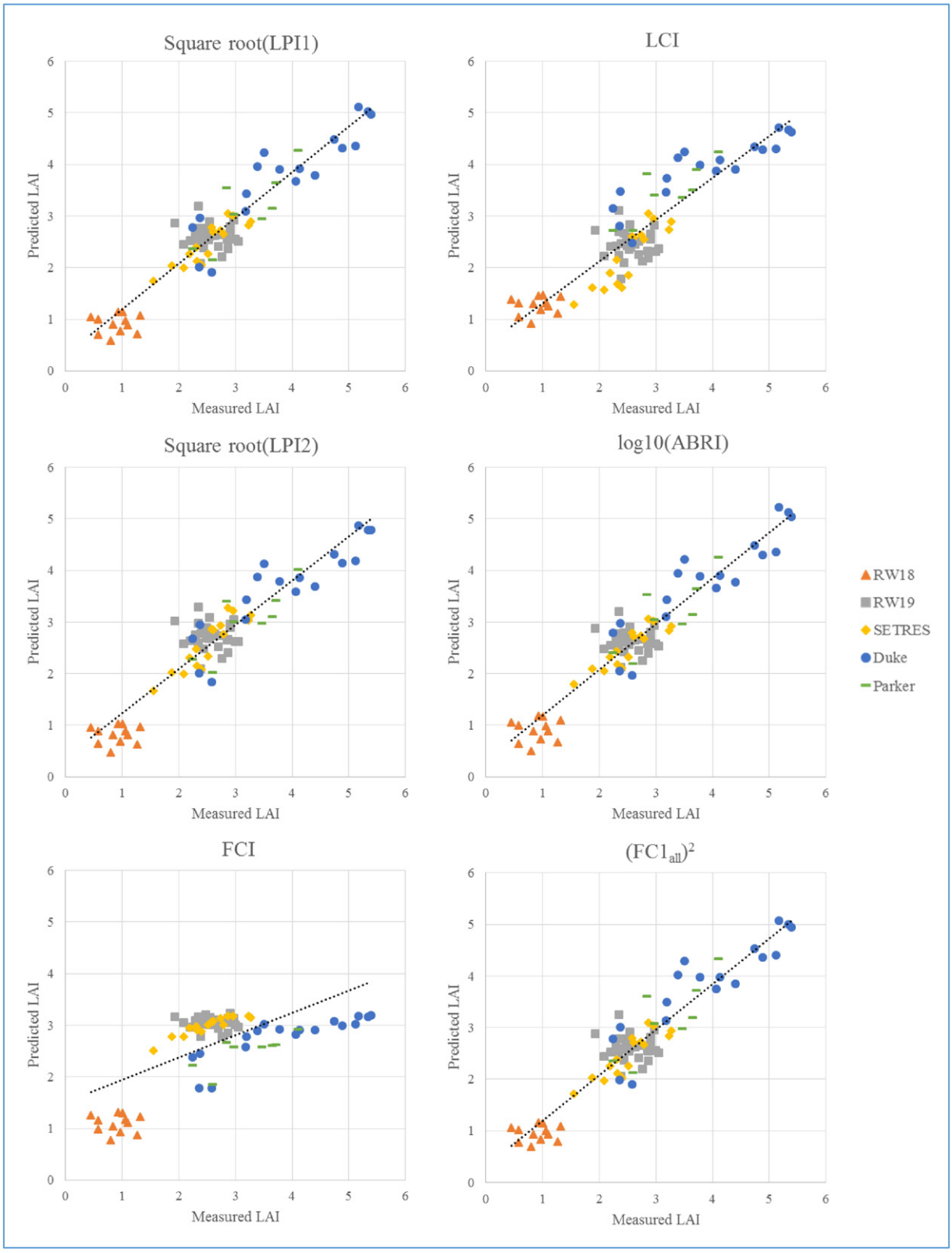

Fig. 1. LiDAR return frequency based indices predicted LAI vs. field measured LAI. Color codes represent the observations from each of the five study sites.

3.3. Combining LiDAR metrics in a single model

When combining all the LiDAR derived indices including the return height and intensity distribution summary statistics the $\log_{10}$ transformed *ABRI* was combined with the coefficient of variation for the C4 crown density bin (LiDAR returns within the 3.5–4.5 m bin above return frequency mode height) ($C4_{cv}$) and the skewness of vegetation return intensity ($Int_{veg.skew}$). The regression equation was as

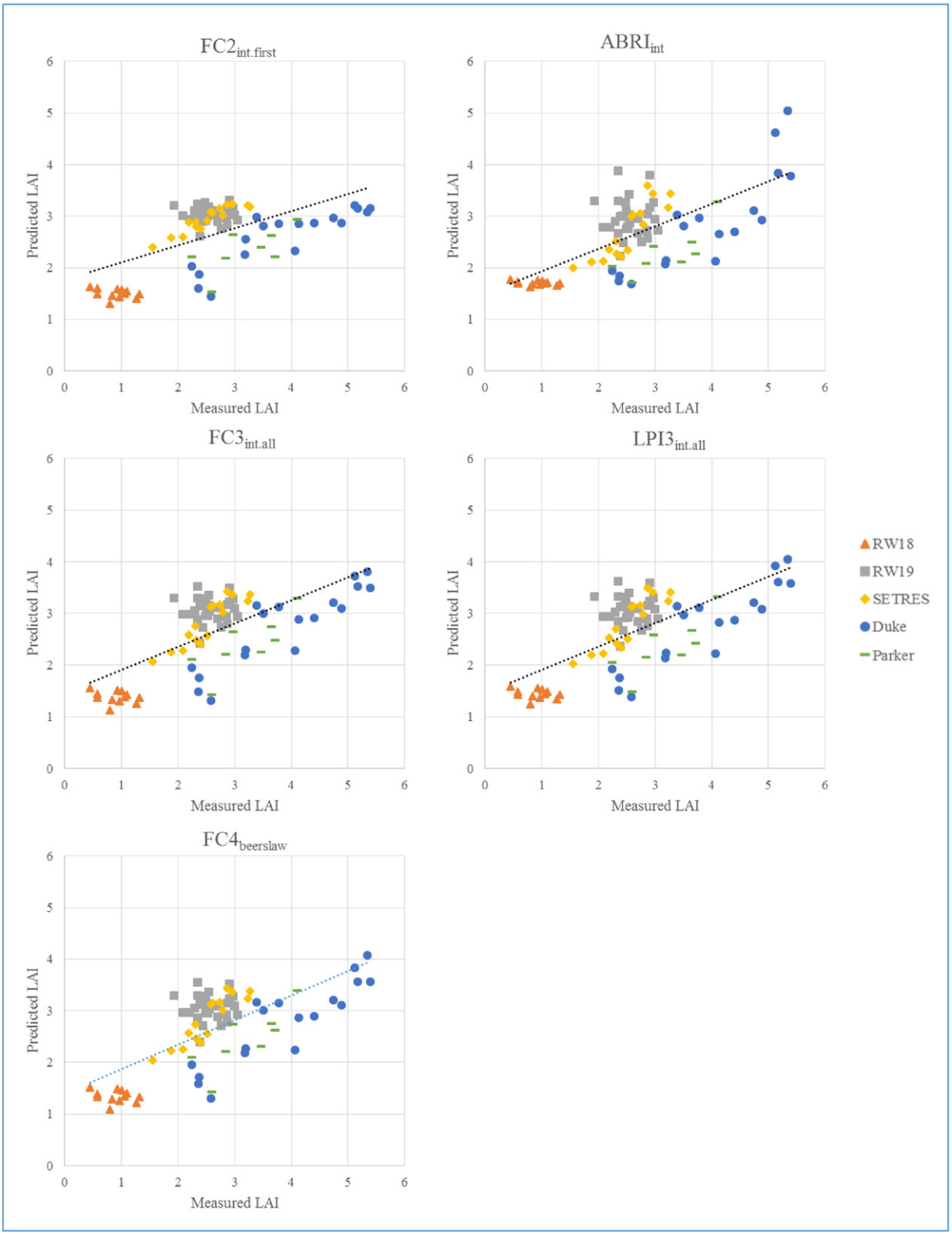

Fig. 2. LiDAR return intensity sum based indices predicted LAI vs. field measured LAI. Color codes represent the observations from each of the five study sites.

follows:

$$LAI_{pred} = 1.738 + 3.539 \times \log_{10}(ABRI) - 0.158 \times C4_{cv} + 0.275 \times Int_{veg.skew} \quad (2)$$

where LAI_{pred} is predicted LAI. The model produced an R^2 value of 0.898 (adj. R^2 0.894) with a standard error of 0.345, (see Fig. 4). The R^2 value for the three predictor model produced a slightly higher R^2 and lower standard error value when compared with the single predictor model

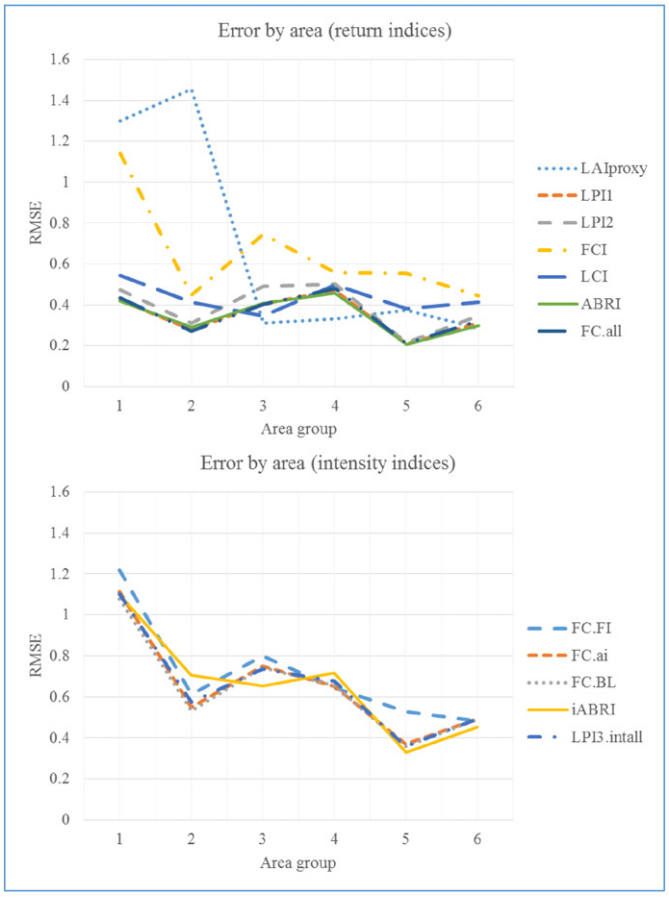

Fig. 3. RMSE values from LiDAR index models calculated for groups of plot sizes (1–6). These groups were: (1) 225–399 m^2; (2) 400–499 m^2; (3) 600–699 m^2; (4) 700–799 m^2; (5) 900 m^2 and (6) 1200–1299 m^2.

including the log_{10} transformed ABRI, where R^2 varied by 0.012 and standard error varied by 0.015.

3.4. Index bivariate correlation analysis

A matrix of the bivariate Pearson correlation relationships are summarized in Table 5. Overall, with the exception of the LAI_{PROXY} index, all bivariate relationships are significantly correlated ($p < 0.01$). The poorest correlations existed for the LAI_{PROXY} index, with a number of non-significant ($p > 0.05$) relationships between $ABRI_{int}$ and *LPI*2, in addition to three lower significance relationships ($p < 0.05$) with *FCI*1, *LPI*1 and *ABRI*. Higher correlations for the LAI_{PROXY} were observed for those indices derived from intensity (except $ABRI_{int}$) and two return frequency based indices (*FCI* and *LCI*).

High correlations were observed in-between those indices derived from intensity information producing high Pearson coefficient values ($r > 0.84$). Intensity indices correlated with return frequency indices typically in the range of $r = 0.63$ to 0.76. Two indices, however, the *FCI* and *LPI*2 produced *r* values between 0.75 and 0.95. The *LCI* correlated relatively poorly with the intensity indices with *r* values in the range of 0.43 to 0.58. Those indices computed from the frequency of LiDAR returns were very highly correlated with one another, and with the exception of the *FCI* and LAI_{PROXY}, Pearson correlation (*r*) values ranged from 0.9 to 1.0.

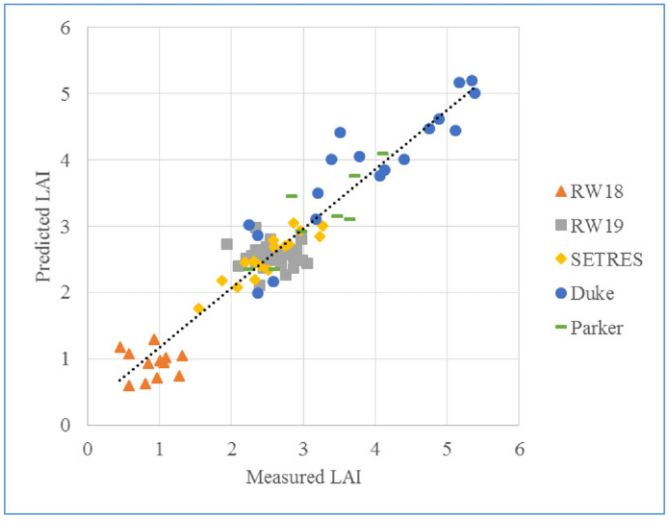

Fig. 4. Graph of field measured LAI against LAI predicted from three LiDAR derived metrics (see Eq. (2)).

4. Discussion

4.1. Testing of predictive models

The current study has tested a number of LiDAR derived indices used to predict LAI for forested environments after calibration of the regression models with field data of variable plot size. Overall the prediction results for the majority of the models utilizing all-return frequencies are in line with the theory and results presented in previous studies (e.g. Morsdorf et al., 2006; Solberg et al., 2009). A number of these LiDAR indices failed or produced a poor relationship with field measured LAI however.

The group of indices which produced the highest correlation with field measured LAI were based upon the frequency of LiDAR returns within different portions of the forest vertical profile. The highest correlations were calculated from those indices which used all returns. Those indices which stratified between single, first, and last returns produced poorer results (i.e. LAI_{PROXY}, *FCI* and *LCI*). Morsdorf et al. (2006) reported an R^2 for their implementation of LAI_{PROXY} as 0.69, which is substantially different to that reported within the current project (R^2 0.07). It should be noted that Morsdorf et al. (2006) developed the index for study sites containing forest species and located within geographic locations not encountered within the current project, in addition to using different data acquisition parameters. Korhonen et al. (2011) reported lower standard error for LAI estimates derived through *FCI* (0.56) when compared to the results presented here (0.81). The authors also present a standard error of 0.45 for estimates using the LCI, which was comparable to results of the current study (0.46). With the exception of LAI_{PROXY}, which failed to produce a correlation, the *FCI* and *LCI* exhibited distributions, when plotted, which are indicative of multiple populations (see Fig. 1). These groups seem to separate by study site, where SETRES and RW19 (2008 acquisition) differ from similar LAI values recorded for Duke and Parker (2013) datasets.

Non-linear relationships were identified in the remaining four return frequency based indices. Barilotti et al. (2005) reported an R^2 value of 0.89 when employing the *LPI*1 in linear regression modeling against LAI values within a range of 3 and 6. A similar level of correlation was observed in the current study (R^2 0.89), however a non-linear transformation was required within the regression model. Solberg et al. (2009) reported R^2 values of 0.93 for the *LPI*2 over a similar range of LAI values to the current study for sites in the Østmarka forest, Norway, dominated by Norway spruce. The implementation of *LPI*2 here returned a similar R^2 value of 0.86. Estimates using the *LPI*2 within the study by Korhonen et al. (2011) report a standard error of 0.38, which are again comparable with 0.40 here. However, as described above, the transformed *LPI*2 underestimated LAI values in the upper portions of the LAI range observed (i.e. >4). The regression model for the log_{10} transformed *ABRI* returned an R^2 value of 0.89 which was higher than that presented in

Table 5
Pearson correlation matric of LiDAR LAI related indices. Pearson coefficients (*Pearson*) and two-tailed significance (*sig.*) are listed for each bivariate correlation. '*' indicate a significance of <0.05, and '**' indicate a significance of <0.01.

		$FC2_{.in,first}$	$FC3_{.int.all}$	$LPI3_{.int.all}$	$FC4_{.beerslaw}$	$ABRI_{.int}$	*FCI*	*LCI*	LAI_{PROXY}	$(FC1_{.all})^2$	*sqrt*(*LPI*1)	*sqrt*(*LPI*2)	$\log_{10}$(*ABRI*)
$FC2_{.in,first}$	*Pearson*	1	.972**	.955**	.962**	.842**	.954**	.434**	.533**	.630**	−.638**	−.721**	.645**
$FC3_{.int.all}$	*Pearson*		1	.997**	.998**	.928**	.917**	.559**	.368**	.728**	−.733**	−.801**	.738**
$LPI3_{.int.all}$	*Pearson*			1	.997**	.955**	.890**	.564**	.334**	.728**	−.733**	−.798**	.737**
$FC4_{.beerslaw}$	*Pearson*				1	.938**	.911**	.584**	.338**	.747**	−.752**	−.816**	.757**
$ABRI_{.int}$	*Pearson*					1	.753**	.568**	.188	.706**	−.710**	−.758**	.714**
FCI	*Pearson*						1	.540**	.474**	.714**	−.723**	−.797**	.732**
LCI	*Pearson*							1	−.477**	.961**	−.957**	−.930**	.952**
LAI_{PROXY}	*Pearson*								1	−.257*	.243*	.142	−.229*
$FC1_{.all.sq}$	*Pearson*									1	−1.00**	−.990**	.998**
sqrt(*LPI*1)	*Pearson*										1	.991**	−1.00**
sqrt(*LPI*2)	*Pearson*											1	−.992**
$\log_{10}$(*ABRI*)	*Pearson*												1

Sumnall et al. (2016) (R^2 of 0.74–0.77) which employed the 2013 dataset used within the current study. The increased correlation coefficient value no doubt corresponds to the increased number of samples employed within the model (Strunk, Temesgen, Andersen, Flewelling, & Madsen, 2012) covering a wider range of LAI values. The $FC1_{all}$ index has been correlated in previous studies with fractional cover rather than LAI, however there are parallels between the two descriptive site values as they both incorporate the Beer–Lambert law of light attenuation (Hopkinson & Chasmer, 2009). The transformed version of the $FC1_{all}$ index within this study produced a strong linear correlation with LAI of R^2 0.88, but under- or over-estimates LAI values less than one or greater than four, respectively. Part of the $FC1_{all}$ model, the constant/intercept was not significant, indicating that if the index value is zero, that the predicted LAI value will not significantly differ from zero.

The models utilizing the sum of intensity all produced poor results overall in terms of R^2 (0.33–0.48) and standard error value (0.77–0.87), especially when compared to an all-return based index. The models developed consistently underestimated LAI values. Whilst not a direct comparison, Hopkinson and Chasmer (2009) incorporated LiDAR intensity within a number of indices in order to estimate fractional cover (see Table 3) for seven study sites in Canada and including a number of different species types. The authors reported the intensity based models produced the highest correlations (R^2 0.75–0.78), when compared to indices based upon the frequency of LiDAR returns (R^2 0.70–0.74).

The multi-predictor model incorporating the $\log_{10}$ transformed *ABRI*, canopy density slice and skewness of intensity values did not increase the R^2 value (+0.012) or decrease standard error value (−0.015) a great deal when considering the single predictor model. There appears to be little benefit to including such additional predictor metrics.

4.2. Consideration of sensor and survey construction differences

The size of the area in which to estimate LAI is also of significance. There are a number of examples in the literature providing experiential evidence about the importance of plot size (e.g. Zhao & Popescu, 2009; Morsdorf et al., 2006; Richardson et al., 2009). Plot size within the current project was not consistent and varied from 225 m^2 to 1280 m^2. The standard error and plot area classified RMSE appears consistent in a number of models (*LPI*1, *LPI*2, *ABRI* and $FC1_{all}$) which provided the highest correlation, for all study sites and datasets, indicating that the influence of plot size was relatively low within the current context. The other indices tested, however, namely the FCI and all intensity based indices appear to be sensitive to plot size (see Fig. 3), where RMSE is largest in small plot sizes and decreases for larger areas and is more variable between groups, whilst all RMSE values are still inferior to the all-return based indices. It should be considered, however, the smallest plot sizes (class 1) were from the 2013 acquisition, whilst the remainder was from 2008, where the trends observed may be related to the two populations observed in Fig. 2, and the number of plots in each area classification varied from 8 to 45, both of which represent a possible source of bias. The results, however, imply the position that all-return based indices are less limited in terms of transferability to other study designs.

Setting an appropriate height threshold for the separation of ground and vegetation returns was found to be optimal as the set up height of the LAI 2200 instrument in the study presented in Sumnall et al. (2016). Zhao and Popescu (2009) report, however, that this may not be optimal if using hemispherical photographs.

The initial field estimation of LAI is subject to a number of uncertainties (Dewey, Roberts, & Hartley, 2006), due to the assumptions within the algorithm applied to model LAI relating to the separation of leaves from woody objects and consideration of foliage clustering. Further considerations arise from field based estimates of LAI from optical instruments, which operate upon measurements from an angular field of view from a point (Varhola, Frazier, Teti, & Coops, 2012), which are often recorded and averaged for an area, which is in contrast to the downward vertical sampling of foliage from airborne LiDAR. No information is available to define how far and what an optical sensor can detect when taking measurements for the indirect estimation of LAI. For example within the current study the LiCOR 2200 was used with a 90° view cap, effectively removing information from other directions. Such a device will also "see" further in more open canopies and a shorter distance in in thicker canopies of high LAI (Zhao & Popescu, 2009), a situation which may be further complicated in more structurally complex or heterogeneous stands.

The current study has tested a number of indices cited in the related literature as having the potential to predict LAI for forested environments once calibrated. A number of trends are evident from the analysis presented here, where the models which were most highly correlated with field recorded LAI were calculated from the sum of all LiDAR returns. Those models which produced low correlations or exhibited patterns where there were distinct groups when viewed graphically were constructed using combinations of first, last or single returns, or used the sum of return intensity. In reference to Fig. 1, the *FCI* exhibits at least two non-linear populations in addition to a cluster of lower values corresponding to those records from RW18. The graphical output for the *LCI* appears to show two populations corresponding to the datasets from 2008 for lower values of LAI and 2013 for higher values. The index *LPI*2 utilizes single, first and last returns within its calculation, but does not exhibit patterns within the predicted values, it does however underestimate higher values of LAI, i.e. those encountered in the sites recorded in 2013. This implies that there is a disparity between the proportions of first, last or single returns recorded by the two different sensors in the separate 2008 and 2013 acquisitions, therefore, methods based on such approaches cannot be transferred to other sites or acquisition parameters.

These two distinct sensors will have a different sensitivity to the detection of multiple features per pulse (Naesset, 2009; Hopkinson, 2006), thus the proportions of first-of-many, single and last returns will differ when comparing systems capable of detecting differing types of returns. The Optech ALTM 3100 system could record up to four returns per pulse, whereas the Riegl VQ-480 could record up to six. The sensor pulse frequency also differs between the two acquisitions (70 kHz and 150 kHz). Hopkinson and Chasmer (2009) investigated the differences in sampling density and reported that models constructed from return frequency ratios (e.g. $FC1_{all}$) could produce comparatively higher estimates of fractional cover at lower frequencies. Thus, a lower frequency of sampling would result in a systematically higher number of returns recorded within the upper forest canopy than for a higher sampling frequency. It should be noted that the investigation in Hopkinson and Chasmer (2009) was applied to a single study site, the observations may not be applicable across all other potential sites and acquisitions. There were no appreciable differences in estimates between the two datasets which utilized all the LiDAR returns within this current project when LAI ranges overlapped (e.g. *ABRI* and *LPI*1). Indices using first returns, such as the *FCI*, express similarities to the phenomena described above, especially for the SETRES and RW19 sites. These issues appear symptomatic of locational or data acquisition specific differences which may pose problems to the transferability of LiDAR based LAI models, in particular those employing the ratios of different return types. Future studies should test those models identified within the current study for their validity in different forest types and geographical locations.

Hopkinson and Chasmer (2009) also stated that indices calculated from intensity were not affected by the frequency of the sampling or pulse power. Within the current project, however, indices calculated from intensity performed poorly and when plotted revealed the presence of two populations with linear or non-linear appearance for the SETRES and RW19 sites (from 2008) and the Duke and Parker sites (from 2013) over a similar range of LAI values. It should also be noted that the two systems used a different wavelength for the laser pulse within the current study, where differences in laser reflection properties resulting in 'brighter' returns at different wavelengths could account for some differences (Li et al., 2013). The storage of the recorded intensity values also differed between the 2008 and 2013 datasets, resulting in the latter having a lower resolution dataset. The usage of LiDAR intensity remains a contested issue due to the proprietary methods that commercial sensors use to report return intensity which can change in flight, making it impossible to directly compare two returns, such as the reflectivity of the target and the amount of the pulse interacting with the target (Lim et al., 2003a). Unless some technique of calibrating intensity values is applied to the data acquired from different acquisitions, the transferability of such models does not appear to be possible.

4.3. Implications and considerations

The LiDAR sensor emits numerous near-infrared pulses, where some will be reflected from the canopy and some will reach the ground. Fundamentally, the ratio of how many returns are from the ground and how many are returned from on or within the canopy has shown to be directly related to plant area and therefore leaf area.

Each of the LiDAR indices used within the current project share similarities in terms of their calculation, where the number or sum of intensity values of ground, canopy and all returns are ratioed against one another. The similarity in terms of information content is further exemplified when considering the bivariate correlation matrix presented in Table 5, where significant ($p < 0.01$) relationships existed for all the indices, with the exception of LAI_{PROXY}. High correlations were found between intensity based indices and the *FCI*, which was calculated from the ratio of first returns, which is unsurprising given the similarity in the pattern of values (see Figs. 1 and 2). High correlation values existed for many of the bivariate relationships, which was especially evident between those indices using return frequency. Those highest correlations were recorded for *ABRI*, $FC1_{all}$, *LPI*1, and even *LCI* when considering the issues mentioned previously. Each of these indices also provided the highest correlation with field LAI. Where each of these indices ratio different components (ground, canopy and all returns) and work for all practical purposes, and thus equate to the same thing.

The results of the current study illustrate the differences in LiDAR sensors and the issues relating to the methods each system uses to record data for analysis. The differences encountered between the proportions of return types (e.g. first, last) and intensity values imply that methods using this data are critically limited in terms of their transferability to other LiDAR acquisitions. The use of indices calculated from all-returns, however, appears compatible with different LIDAR sensor datasets, and therefore are potentially transferable, at least for Loblolly pine forest.

Parallels can be drawn to the model development of optical-spectral indices which are often used to estimate LAI, where many indices are calculated from a ratio or difference between different portions of the reflected spectrum of electromagnetic radiation (Bannaria, Morina, Bonna, & Hueteb, 1995), for example the red edge and the chlorophyll trough, with one such example being the Normalized Difference Vegetation Index (NDVI). For homogenous closed stand conditions, it makes little difference which vegetation index used to estimate LAI because they are all fundamentally linked to the same thing (Broge & Leblanc, 2001). Thus, the argument can be made that a similar level of maturity has been achieved with respect to the estimation of LAI using the LiDAR return frequency based indices (all returns) as with spectral vegetation indices, such as the NDVI and its variants.

Overall, techniques such as the use of spectral indices can approximate LAI for canopies with LAI in the range of 3–5 (Chen & Chilar, 1996, Turner, Cohen, Kennedy, Fassnacht, & Briggs, 1999). Issues arise for values above this LAI threshold, as many indices saturate causing LAI estimates for high biomass to be incorrectly estimated. The spatial resolution of satellite imagery, especially, can lead to the mixture of surface cover types into a single value, for example thinned and open plot understory and ground reflectance can adversely affect estimates of LAI. While the saturation of LiDAR derived indices is possible, the results presented in the current study suggest LiDAR estimates of LAI are not as limited by saturation effects and can estimate LAI values over a range between zero to in excess of five, at relatively small spatial resolutions, which are also less sensitive to understory presence and are less subject to the increases error associated with thinned and open areas within a forest context. In addition, the link between field LAI measurement height and the threshold of what defined 'ground' and 'canopy' within LiDAR returns, as suggested in Sumnall et al. (2016), implies that estimates of the vertical distribution of LAI vertically through the canopy is possible.

In densely vegetated forest environments there is the possibility that no LiDAR laser pulses will penetrate and return from the depth required for the computation of the index, which would result in inaccurately predicting the LAI value. A parallel can be drawn from vegetation indices developed for multispectral data, such as the NDVI which saturate at higher LAI values (Wang, Adiku, Tenhunen, & Granier, 2005). The inclusion of the scanning angle of each laser pulse could be incorporated in the model construction, as at larger scanning angles the laser pulse may penetrate through gaps which would not be possible at near-nadir angles (Richardson et al., 2009), although additional concerns relating to scan length, pulse energy and light attenuation would need to be addressed. The likelihood of increasing the number of returns from the lower portions of the LiDAR vertical profile potentially increases with larger plot size. Advances in small-footprint LiDAR technologies, such as full-waveform retrieval, could potentially provide a greater number of returns per pulse (Chauve et al., 2007) and reduce an issue prevalent in discrete return LiDAR, where there is a 'blind spot' following each detected return (up to 1.2–5 m), during which nothing can be detected (Reitberger et al., 2008).

The current study included a range of Loblolly pine stands with differing management types applied, some of which included understory control. A number of these stands, in particular Duke or Parker Tract, included a number of multiple vertical layers, where both coniferous and deciduous species were present in the shrub, understory and mid-story layers beneath the dominant canopy. The presence and absence of vegetation within these layers will influence the total LAI of a given area, and will alter throughout the year in temperate regions. Given LiDARs ability to penetrate the canopy and estimate the presence of sub-canopy features (e.g. Hill & Broughton, 2009), future work could attempt to estimate the presence of these layers and the potential influence upon area-total LAI they have.

5. Conclusions

The application of airborne LiDAR for estimating LAI can provide a number of benefits in comparison to the analysis of optical multispectral data in terms of accuracy and scale, particularly in areas of medium to high biomass and were forest canopy cover is not uniform over large areas. The current study demonstrates the usefulness of a number of LiDAR derived indices calculated from the ratio of returns from different portions of the vertical return information provided, for predicting LAI from multiple datasets from Loblolly pine dominated forest of homogeneous canopy types. The investigated predictors included a variety of laser-penetration indices using either frequency of return or the sum of return intensity over a variety of stand ages, forest management conditions and geographical locations.

The non-linear transformed $\log_{10}$ *ABRI* and square root transformed *LPI*1 have demonstrated the strongest correlations with field estimates of LAI, by LAI 2000/LAI 2200. The addition of other LiDAR derived return frequency or intensity distribution did not improve prediction accuracy to any great degree. These indices are capable of predicting LAI across two disparate sensor or data acquisition configurations, and offer the potential of a transferable model, at least for managed Loblolly pine sites. Those indices derived from single, first-of-many and last returns or the sum of return intensities consistently produced inferior correlations and exhibited a number of differences in terms of value distribution which indicates separate populations corresponding to the data from the two separate LiDAR acquisitions, in addition to concerns over sensitivity to plot size. This implies that indices developed using such data from disparate LiDAR sensor or data acquisition configurations are not transferable. Alternatively, it suggests that such indices should be calibrated independently for each change in survey configuration.

Many of the LiDAR derived indices were highly correlated with one another. Those indices derived from the frequency of all LiDAR returns in particular (e.g. *LPI*1 and *ABRI*), all used ratios of returns from different vertical parts of the canopy, but ultimately produced very similar results in terms of predicted LAI. This indicates a similar level of development to multispectral indices for the estimation of LAI.

The results of the current study offer the potential to estimate LAI robustly from airborne LiDAR data consistently when employing multiple sensor or data acquisition configurations for managed Loblolly pine stands at various field-plot scales. This may hold the potential for reducing the need to calibrate LiDAR data against field measured LAI in the future. There is a great deal of disparity within the current literature regarding the estimation of LAI from LiDAR however, with the metrics used in many studies which are site specific (Zhao & Popescu, 2009). At this stage it may be premature to state that there is one 'ideal' model for estimating LAI, thus future work should place an emphasis on assessing the transferability of published methods to new geographic contexts, sensor types and survey characteristics. In addition given LiDARs ability to penetrate through the dominant canopy and identify sub-canopy features it may be possible to estimate how LAI changes throughout the vertical profile, and what the data requirements of this might be.

Acknowledgments

This research was possible thanks to the support from the Forest Productivity Cooperative, the help in field data collection provided by Beth Stein and the assistance Alica Peduzzi, who provided the field data for validation of the 2008 LiDAR acquisition assessed in the project. We gratefully acknowledge the support and LiDAR data supplied by NASA, in addition to the support of the staff members of the Duke Forest teaching and research laboratory, the Northern Research Station Strategic Foresight Group of the North Carolina Forest service and the landowner Weyerhaeuser. Funding for this work was provided in part by the Virginia Agricultural Experiment Station (Project Number VA-136623) and the Program McIntire Stennis of the National Institute of Food and Agriculture, U.S. Department of Agriculture.

References

Anderson, J. E., Plourde, L. C., Martin, M. E., Braswell, B. H., Smith, M. L., Dubayah, R. O., ... Blair, J. B. (2008). Integrating waveform LiDAR with hyperspectral imagery for inventory of a northern temperate forest. *Remote Sensing of Environment*, *112*(4), 1856–1870.

Albaugh, T. J., Allen, H. L., Dougherty, P. M., Kress, L. W., & King, J. S. (1998). Leaf area and above- and belowground growth responses of Loblolly pine to nutrient and water additions. *For. Sci.*, *44*, 317–328.

Armston, J. (2014) RSC Las Tools - version 1.9.3 [Computer program] Available from: <https://code.google.com/p/rsclastools/>.

Bannaria, A., Morina, D., Bonna, F., & Hueteb, A. R. (1995). A review of vegetation indices. *Remote Sensing Reviews*, *13*(1–2), 95–120.

Barilotti, A., Turco, S., Napolitano, R., & Bressan, E. (2005). La tecnologia LiDAR per lo studio della biomassa negli ecosistemi forestali. *15th Meeting of the Italian Society of Ecology, Torino, Italy*.

Bioucas-Dias, J. M., Plaza, A., & Dobigeon, N. (2012). Hyperspectral unmixing overview: Geometrical, statistical, and sparse regression-based approaches. *IEEE Journal of Selected Topics in Applied Earth Observations and Remote Sensing*, *5*(2), 354–379.

Bowerman, B. L., & O'Connell, R. T. (1990). *Linear statistical models: An applied approach* (2nd ed.). Belmont, CA: Duxbury.

Broge, N. H., & Leblanc, A. (2001). Comparing prediction power and stability of broadband and hyperspectral vegetation indices for estimation of green leaf area index and canopy chlorophyll density. *Remote Sensing of Environment*, *76*(2), 156–172.

Chauve, A., Mallet, C., Bretar, F., Durrieu, S., Deseillgny, M., & Puech, W. (2007). Processing full-waveform lidar data: Modelling raw signals. *International Archives of Photogrammetry, Remote Sensing and Spatial Information Sciences*.

Chen, J. M., & Black, T. A. (1992). Defining leaf area index for non-flat leaves. *Plant cell and environment.*, *15*, 421–429.

Chen, J., & Chilar, J. (1996). Retrieving leaf area index of boreal forests using Landsat TM images. *Remote Sensing of Environment*, *55*, 153–162.

Chen, J. M., Chen, X. Y., Ju, W. M., & Geng, X. Y. (2005). Distributed hydrological model for mapping evapotranspiration using remote sensing inputs. *Journal of Hydrology*, *305*, 15–39.

Cleugh, H. A., Leuning, R., Mu, Q., & Running, S. W. (2007). Regional evaporation estimates from fluxtower and MODIS satellite data. *Remote Sensing of Environment*, *106*, 285–304.

Cook, B. D., Corp, L. W., Nelson, R. F., Middleton, E. M., Morton, D. C., McCorkel, J. T., ... Montesano, P. M. (2013). NASA Goddard's LiDAR, Hyperspectral and Thermal (G-LiHT) airborne imager. *Remote Sensing*, *5*, 4045–4066.

Dewey, J. C., Roberts, S. D., & Hartley, I. (2006). A comparison of tools for remotely estimating Leaf area index in Loblolly pine plantations. In K. F. Connor (Ed.), *Proceedings of the 13th biennial southern silvicultural research conference Gen. Tech. Rep. SRS92 (pp. 77–75) Ashville, NC: US Dept. of Agriculture, Forest service, southern research station* (pp. 640).

Duchemin, B., Hadriab, R., Errakib, S., Bouleta, G., Maisongrandea, P., Chehbounia, A., ... Simonneauxa, V. (2006). Monitoring wheat phenology and irrigation in: Central Morocco: On the use of relationships between evapotranspiration, crops coefficients, leafarea index and remotely-sensed vegetation indices. *Agricultural Water Management*, *79*, 1–27.

Erikson, H. M., Eklundh, L., & Kuusk, T. (2006). Impact of understory vegetation on forest canopy reflectance and remotely sensed LAI estimates. *Remote Sensing of Environment*, *103*, 408–418.

Evans, J. S., Hudak, A. T., Faux, R., & Smith, A. M. S. (2009). Discrete return LiDAR in natural resources: Recommendations for project planning, data processing, and deliverables. *Remote Sensing*, *1*(4), 776–794.

Falkowski, M. J., Evans, J. S., Martinuzzi, S., Gessler, P. E., & Hudak, A. T. (2009). Characterizing forest succession with LiDAR data: An evaluation for the inland northwest, USA. *Remote Sensing of Environment*, *113*(5), 946–956.

Field, A. (2013). *Discovering statistics using SPSS* (4th ed.). California, USA: SAGE Publications Ltd.

Hill, R. A., & Broughton, R. K. (2009). Mapping the understorey of deciduous woodland from leaf-on and leaf-off airborne LiDAR data: A case study in lowland Britain. *ISPRS Journal of Photogrammetry and Remote Sensing*, *64*(2), 223–233.

Hopkinson, C. (2006). The influence of LiDAR acquisition settings on canopy penetration and laser pulse return characteristics. *Proceeding of: Geoscience and Remote Sensing Symposium*.

Hopkinson, C., & Chasmer, L. (2009). Testing LiDAR models of fractional cover across multiple forest ecozones. *Remote Sensing of Environment*, *113*, 275–288.
Hudak, A. T., Crookston, N. L., Evans, J. S., Hall, D. E., & Falkowski, M. J. (2008). Nearest neighbor imputation of species-level, plot-scale forest structure attributes from LiDAR data. *Remote Sensing of Environment*, *112*(5), 2232–2245.
Kaartinen, H., Hyyppa, J., Yu, X. W., Vastaranta, M., Hyyppa, H., Kukko, A., ... Wu, J. C. (2012). An international comparison of individual tree detection and extraction using airborne laser scanning. *Remote Sensing*, *4*(4), 950–974.
Korhonen, L., Korpela, I., Heiskanen, J., & Maltamo, M. (2011). Airborne discrete-return LiDAR data in the estimation of vertical canopy cover, angular canopy closure and leaf area index. *Remote Sensing of Environment*, *115*, 1065–1080.
Lefsky, M. A., Cohen, W. B., Parker, G. G., & Harding, D. J. (2002). LiDAR remote sensing for ecosystem studies. *Bioscience*, *52*(1), 19–30.
Leuning, R., Cleugh, H. A., Zegelin, S. J., & Hughes, D. (2005). Carbon and water fluxes over a temperate Eucalyptus forest and a tropical wet/dry savanna in Australia: Measurements and comparison with MODIS remote sensing estimates. *Agricultural and Forest Meteorology*, *129*, 151–173.
Li, Z., Douglas, E., Strahler, A., Schaaf, C., Yang, X. Y., Wang, Z. S., ... Lovell, J. L. (2013). Separating leaves from trunks and branches with duel-wavelength terrestrial LiDAR scanning. *IEEE International Symposium on Geoscience and Remote Sensing IGARSS. Melbourne, Australia* (pp. 3383–3386).
Lim, K., Treitz, P., Baldwin, K., Morrison, I., & Green, J. (2003a). LiDAR remote sensing of biophysical properties of tolerant northern hardwood forests. *Canadian Journal of Remote Sensing*, *29*(5), 658–678.
Lim, K., Treitz, P., Wulder, M., St-Onge, B., & Flood, M. (2003b). LiDAR remote sensing of forest structure. *Progress in Physical Geography*, *27*(1), 88–106.
Maltamo, M., Packalen, P., Yu, X., Eerikainen, K., Hyyppa, J., & Pitkanen, J. (2005). Identifying and quantifying structural characteristics of heterogeneous boreal forests using laser scanner data. *Forest Ecology and Management*, *216*(1–3), 41–50.
Morsdorf, F., Kötz, B., Meier, E., Itten, K. I., & Allgöwer, B. (2006). Estimation of LAI and fractional cover from small footprint airborne laser scanning data based in gap fraction. *Remote Sensing of Environment*, *104*, 50–61.
Næsset, E. (2002). Predicting forest stand characteristics with airborne scanning laser using a practical two-stage procedure and field data. *Remote Sensing of Environment*, *80*(1), 88–99.
Naesset, E. (2009). Effects of different sensors, flying altitudes, and pulse repetition frequencies on forest canopy metrics and biophysical stand properties derived from small-footprint airborne laser data. *Remote Sensing of Environment*, *113*, 148–159.
Peduzzi, A., Wynne, R. H., Thomas, V. A., Nelson, R. F., Reis, J. J., & Sanford, M. (2012a). Combined use of airborne LiDAR and DBInSAR data to estimate LAI in temperate mixed forests. *Remote Sensing*, *4*(6), 1758–1780.
Peduzzi, A., Wynne, R. H., Fox, T. R., Nelson, R., & Thomas, V. A. (2012b). Estimating leaf area index in intensively managed pine plantations using airborne laser scanner data. *Forest Ecology and Management*, *270*, 54–65.
Reitberger, J., Krzystek, P., & Stilla, U. (2008). Analysis of full waveform LiDAR data for the classification of deciduous and coniferous trees. *International Journal of Remote Sensing*, *29*(5), 1407–1431.
Richardson, J., Moskal, M., & Kim, S. (2009). Modeling approaches to estimate effective leaf area index from aerial discrete return LiDAR. *Agricultural and Forest Meteorology*, *149*, 1152–1160.
Solberg, S., Brunner, A., Hanssen, K. H., Lange, H., Næsset, E., Rautiainen, M., & Stenberg, P. (2009). Mapping LAI in Norway spruce forest using airborne laser scanning. *Remote Sensing of Environment*, *113*, 2317–2327.
Stenberg, P. (1996). Correcting LAI-2000 estimates for the clumping of needles in shoots of conifers. *Agricultural and Forest Meteorology*, *79*, 1–8.
Strunk, J., Temesgen, H., Andersen, H. E., Flewelling, J. P., & Madsen, L. (2012). Effects of LiDAR pulse density and sample size on a model-assisted approach to estimate forest inventory variables. *Canadian Journal of Remote Sensing*, *38*(5), 644–654.
Sumnall, M. J., Fox, T. R., Wynne, R. H., Blinn, C., & Thomas, V. A. (2016). Estimating leaf area index at multiple heights within the understorey component of Loblolly pine forests from airborne discrete-return lidar. *International Journal of Remote Sensing*, *37*(1), 78–99.
Turner, D. P., Cohen, W. B., Kennedy, R. E., Fassnacht, K. S., & Briggs, J. M. (1999). Relationship between leaf area index and Landsat spectral vegetation indices across three temperate zone sites. *Remote Sensing of Environment*, *70*, 52–68.
Varhola, A., Frazier, G. W., Teti, P., & Coops, N. C. (2012). Estimation of forest structure metrics relevant to hydrological modelling using coordinate transformation of airborne laser scanning data. *Hydrology and Earth System Sciences*, *16*, 3749–4376.
Wang, Q., Adiku, S., Tenhunen, J., & Granier, A. (2005). On the relationship of NDVI with leaf area index in a deciduous forest site. *Remote Sensing of Environment*, *94*(2), 244–255.
Welles, J. M., & Norman, J. M. (1991). Instrument for indirect measurement of canopy architecture. *Argon. J.*, *83*, 818–825.
Zhang, K., Chen, S., Whitman, D., Shyu, M., Yan, J., & Zhang, C. (2003). A progressive morphological filter for removing nonground measurements from airborne LiDAR data. *IEEE Transactions on Geoscience and Remote Sensing*, *41*(4), 872–882.
Zhao, K., & Popescu, S. (2009). LiDAR-based mapping of leaf area index and its use for validating GLOBCARBON satellite LAI product in a temperate forest of the southern USA. *Remote Sensing of Environment*, *113*, 1628–1645.